Article

Synergistic Effect of As(III)/Fe(II) Oxidation by *Acidianus brierleyi* and the Exopolysaccharide Matrix for As(V) Removal and Bioscorodite Crystallization: A Data-Driven Modeling Insight

Ricardo Aguilar-López [1] , Sergio A. Medina-Moreno [2], Ashutosh Sharma [3] and Edgar N. Tec-Caamal [3,*]

[1] Department of Biotechnology and Bioengineering, Centre for Research and Advanced Studies of the National Polytechnic Institute, Av. Instituto Politécnico Nacional No. 2508, Mexico City 07360, Mexico
[2] Department of Biotechnology, Polytechnic University of Pachuca, Ex-Hacienda de Santa Bárbara 43830, Mexico
[3] Centre of Bioengineering, School of Engineering and Sciences, Tecnologico de Monterrey, Campus Querétaro, Av. Epigmenio González 500, Querétaro 76130, Mexico
* Correspondence: edgart@tec.mx

Abstract: Bioscorodite crystallization is a promising process for the proper immobilization of arsenic from acidic metallurgical wastewater, and *Acidianus brierleyi* is an effective archaeon to oxidize Fe(II) and As(III) simultaneously. This paper deals with the development of an experimentally validated mathematical model to gain insight into the simultaneous processes of Fe(II) and As(III) oxidation via microbial cells and the exopolysaccharide (EPS) matrix, As(V) precipitation, and bioscorodite crystallization, which are affected by several factors. After the mathematical structure was proposed, a model fitting was performed, finding global determination coefficients between 0.96 and 0.99 (with p-values < 0.001) for all the variables. The global sensitivity analysis via Monte Carlo simulations allowed us to identify the critical parameters whose sensitivity depends on culture conditions. The model was then implemented to evaluate the effect of cell concentration, Fe(II) and As(III) concentrations (at Fe/As = 1.4), and oxidation rate constants for *A. brierleyi* and the EPS region, noting that these factors play an important role in the process. Our results showed that the proposed model can be used as a robust simulation platform for the further analysis of the bioscorodite crystallization process under extremophilic conditions.

Keywords: iron; arsenic; bioscorodite; modeling; exopolysaccharide matrix; precipitation

1. Introduction

The continuous release of arsenic into the environment due to natural or anthropogenic factors has caused public health concern. Bladder, skin and lung cancer, hypertension, and genetic damage are the main adverse health effects due to long-term exposure to arsenic compounds [1]. Therefore, to remove arsenic from water and meet the recommended limit of arsenic in drinking water (10 μg L^{-1}) [2], several technologies have been developed, such as adsorption, ion exchange, coagulation–flocculation, ultrafiltration, and reverse osmosis [3–5]. Metallurgical industries generate acidic wastewater containing high concentrations of arsenic between 500 and 10,000 ppm, where arsenic is predominantly found in its trivalent form (As(III)) [6,7]. In aqueous solutions under acidic conditions, As(III) is considered more toxic than the pentavalent form (As(V)) due to its higher solubility and mobility [8]. Thus, for the treatment of acidic metallurgical streams, the oxidation of As(III) prior to its immobilization is necessary. As(III) can be oxidized chemically to As(V) by strong oxidizing agents (e.g., hydrogen peroxide, chlorine, ozone), or biologically with thermophilic or acidophilic microbes. *Acidianus brierleyi* is an archaeon capable of simultaneously oxidizing As(III) and Fe(II) in a thermoacidophilic environment [9]. Oxidation

with *Acidianus* is carried out enzymatically, but it has also been observed that this strain is able to produce exopolysaccharides (EPS) and to generate a biofilm (EPS matrix) where oxidation reactions take place [10]. The redox capacity of EPS has also been demonstrated with several microorganisms in the reduction/oxidation of different substances such as U(VI) by *Shewanella oneidensis*, arsenate by *Pseudomonas putida*, positively charged silver ions to silver nanoparticles by *Escherichia coli*, and the diammonium salt of 2,2′-Azino-bis(3-ethylbenzthiazoline-6-sulfonic acid) (ABTS) and nitrate, both with activated sludge EPS [11–13]. EPS production is important for *A. brierleyi* as it provides protection to cells under extreme acidic conditions and contributes to the generation of microbiologically active scorodite crystals through biofilm formation as it can promote nucleation [14]. Once Fe(III) and As(V) are in a solution, they can react under controlled conditions and precipitate as scorodite (FeAsO$_4$·2H$_2$O). The crystallization of scorodite by biological means (known as bioscorodite) has been shown to be a feasible procedure for immobilizing high concentrations of arsenic from acidic wastewater due to its high compactness, low solubility, high arsenic content, and low iron requirements for formation [15,16]. An important aspect in the process is that the effluent can provide the microbes with a suitable growth environment, as they can grow in an acidic environment, at high temperature (70–80 °C), and under atmospheric pressure [17]. It is worth mentioning that the bioscorodite crystallization process can reduce operating costs, since the biooxidation, precipitation and crystallization reactions occur simultaneously in the same reactor [14]. Then, the solids can be easily recovered by sedimentation. From the above, the experimental analysis of scorodite crystallization has focused on the effects of operational factors, such as iron/arsenic (Fe/As) molar ration, pH changes, cell concentration, the addition of seeding materials, and nutritional factors [18,19]. Based on the above, the analysis of controlling factors is of particular interest to find the operating conditions under which the kinetics of biooxidation, precipitation and crystallization can be improved. This task can be addressed by mathematical modeling and simulation tools that provide a better understanding of the process dynamics [20–22]. Experimentally validated models can be used to predict bioreactor performance over a wide range of operating scenarios by performing a simulation analysis that takes into account key factors affecting the overall process [23]. It has been observed that bioscorodite crystallization is controlled by oxidation rate and supersaturation, which in turn depends on culture conditions such as oxygen availability, cell concentration, microbial affinity to substrates, or microbial response to extremophilic environments [23–25].

The objective of this study is to analyze the effect of controlling factors on the simultaneous processes occurring in an aerobic reactor when *Acidianus brierleyi* is used for arsenic fixation as bioscorodite from acidic effluents. A mathematical model is developed and validated with a series of experiments under different conditions. The model describes the oxidation of As(III)/Fe(II) by *Acidianus brierleyi* and the EPS region, arsenic precipitation, and bioscorodite crystallization, which is constructed in terms of Monod kinetics considering Fe(II) and As(III) as limiting substrates. It also considers arsenic precipitation and simulates crystal growth associated with arsenic precipitation. The model is then used to analyze the effects of cell concentration, Fe(II) and As(III) concentrations, and oxidation rate constants for *A. brierleyi* and the EPS region on the overall process.
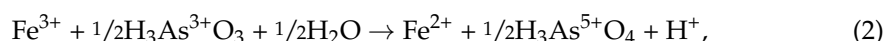
A mathematical model was developed for first time to simulate and analyze the simultaneous processes occurring in the bioscorodite crystallization process under extremophilic conditions for As(III) oxidation and As(V) precipitation, involving the oxidation activity of *Acidianus brierleyi* and the EPS matrix, which can serve as the basis for developing bioreactor design and process optimization approaches.

2. Methodology

2.1. Mathematical Modeling

In this section, we describe a mathematical model able to predict the dynamics of the process involved in the As(V) immobilization as bioscorodite. The industrial application of the bioscorodite crystallization process for arsenic immobilization involves the use of

a series of sequential processes [26]; however, in this work, we focused on the modelling and analysis of the aerobic bioreactor where the As(III)/Fe(II) oxidation–reduction reaction by *Acidianus brierleyi* and by the EPS region, with As(V) precipitation and bioscorodite crystallization, take place simultaneously, as proposed by Okibe et al. [9] (see Figure 1). This process was designed to immobilize high arsenic concentrations from acidic metallurgical wastewaters where arsenic is mainly found in its trivalent form. The process is carried out under a thermoacidophilic environment, where microbial cells oxidize Fe(II) to Fe(III) and As(III) to As(V). Then, Fe(III) and As(V) react to precipitate in the form of biogenic scorodite, which then forms crystals. The model is built considering the following assumptions: (i) The As(III) oxidation activity of *Acidianus brierleyi* is carried out enzymatically but does not promote cell growth, implying the activation of a microbial detoxification mechanism when microbes are exposed to trivalent arsenic (see Equation (1)) [27]; (ii) *A. brierleyi* produces EPS, forming an EPS compartment around the cell surface that facilitates As(III) oxidation coupled with Fe(III) reduction [6,9], according to Equation (2). It is important to note that the chemical oxidation of the As(III)/Fe(III) reduction–coupling reaction in the bulk liquid is very slow; thus, this term was disregarded from the model equations [27].

$$As^{3+} + 1/2O_2 + 2H^+ \rightarrow As^{5+} + H_2O, \tag{1}$$

$$Fe^{3+} + 1/2H_3As^{3+}O_3 + 1/2H_2O \rightarrow Fe^{2+} + 1/2H_3As^{5+}O_4 + H^+, \tag{2}$$
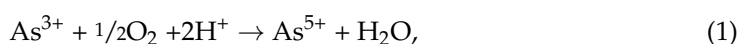
(iii) Fe(II) is oxidized by *A. brierleyi*, where oxygen is the final electron acceptor in the respiratory chain according to Equation (3). Chemical oxidation by dissolved oxygen is not considered in the model equations, as the experimentation indicates that this reaction does not occur in similar systems under high temperature and acid pH [10,14].

$$Fe^{2+} + 1/4O_2 + H^+ \rightarrow Fe^{3+} + 1/2H_2O \tag{3}$$
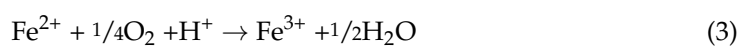
Once Fe(III) is generated in the reactor, this can react with As(V) to precipitate as bioscorodite, according to Equation (4).

$$Fe^{3+} + AsO_4^{3-} + 2H_2O \rightarrow FeAsO_4 \cdot 2H_2O \text{ (Scorodite)} \tag{4}$$
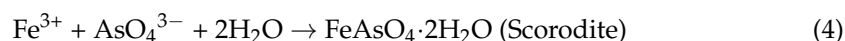
(iv) The pH of the system is considered constant (at pH = 1.5), as experimental observations show slight changes in pH during cultivation [9,27]; (v) oxygen concentration can be considered in excess for metabolic activities [28]; thus, oxygen terms were neglected from the oxidation rate equations; (vi) bioreactors (shaking flasks) were assumed to be isothermal (at 70 °C) and pseudo-homogeneous as a consequence of the hydrodynamic conditions. As indicated by Okibe et al. [27], the experiments were conducted in shaking flasks at 100 rpm, which assumes Reynolds numbers above 4100, indicating turbulent regimes in the vessels. From these considerations, the model equations are deployed below.

Fe(II) oxidation by *Acidianus brierleyi* was modeled based on Monod kinetics, considering Fe(II) as the only limiting substrate as follows:

$$-r_{Fe(II)} = k_{Fe(II)}(C_{bio}) \left(\frac{Fe(II)}{Ks_{Fe(II)} + Fe(II)} \right), \tag{5}$$

where $r_{Fe(II)}$ is the ferrous iron oxidation rate (mmol L^{-1} d^{-1}), $k_{Fe(II)}$ is the Fe(II) oxidation rate constant [mmol d^{-1} (g$_{biomass}$)$^{-1}$], C_{bio} is the biomass concentration [g$_{biomass}$ L^{-1}], and $Ks_{Fe(II)}$ is the affinity constant for Fe(II) [mmol L^{-1}]. In the same sense, the microbial As(III) oxidation can be expressed by Equation (6):

$$-r_{As(III)} = k_{As(III)} \cdot (C_{bio}) \cdot \left(\frac{As(III)}{Ks_{As(III)} + As(III)} \right), \tag{6}$$

where $r_{As(III)}$ is the arsenite oxidation rate (mmol L^{-1} d^{-1}), $k_{As(III)}$ is the As(III) oxidation rate constant [mmol d^{-1} $(g_{biomass})^{-1}$], and $Ks_{As(III)}$ is the affinity constant for arsenite [mmol L^{-1}]. For Equations (5) and (6), it was assumed that biomass concentration is maintained as essentially constant during cultivation, as observed experimentally for iron and arsenite oxidizers [14,28]. However, to analyze the effect of cell concentration on the overall process, C_{bio} was considered in the model equations [29,30]. Considering the EPS region as a transient media for microbial extracellular electron transfer, where the reaction of As(III) oxidation coupled to the Fe(III) reduction takes place, and assuming that the reaction rate is proportional to the product of the concentrations of As(III) and Fe(III) according to the law of mass action, the oxidation–reduction reaction can be represented by Equation (7):

$$- r_{EPS} = k_{EPS}[Fe(III)][As(III)], \tag{7}$$

where r_{EPS} is the oxidation rate for the EPS compartment (mmol L^{-1} d^{-1}), k_{EPS} is the As(III) oxidation rate constant [mmol^{-2} d^{-1}] for the archaeal EPS compartment, Fe(III) is the ferric iron concentration [mmol L^{-1}], and As(III) is the arsenite concentration (mmol L^{-1}). It should be noted that a rate constant has been determined for cytochrome electron transfer in the EPS of the microorganism *Shewanella oneidensis* MR-1 [31]. Based on the above, the classical mass balance approach was used to describe the dynamics of a batch bioreactor.

The mass balance for Fe(II) is given by:

$$\frac{dFe(II)}{dt} = -r_{Fe(II)} + r_{EPS} \tag{8}$$

The mass balance for Fe(III) is expressed by:

$$\frac{dFe(III)}{dt} = r_{Fe(II)} - r_{EPS} - k_{As(V)}[Fe(III)][As(V)] \tag{9}$$

The mass balance for As(III) is defined as:

$$\frac{dAs(III)}{dt} = -r_{As(III)} - \frac{1}{2} \cdot r_{EPS} \tag{10}$$

The mass balance for As(V) is determined by:

$$\frac{dAs(V)}{dt} = r_{As(III)} + \frac{1}{2} \cdot r_{EPS} - k_{As(V)}[Fe(III)][As(V)] \tag{11}$$

where $k_{As(V)}$ is the arsenate precipitation rate constant [L mmol^{-1} d^{-1}].

To analyze the bioscorodite crystallization under thermoacidophilic conditions, the general crystal growth model developed by [32] was used, which only considers crystal growth associated with As(V) precipitation. However, the related biochemical redox reactions and As(V) precipitation dynamics were not considered in the model structure. Thus, in this study, the oxidation and precipitation kinetics were coupled with the model reported by González-Contreras et al. [32]. Briefly, in the crystallization model, mass deposition is assumed to proceed by a diffusion process, where the solute molecules are transported from the liquid phase to the solid phase [33]. The solute molecules are then arranged in a crystalline matrix, which is described by a first-order reaction. The relationship between the mass deposition rate [R_G, kg m^{-2} d^{-1}] and the linear growth rate [$G = dL/dt$, m d^{-1}] is given by Equation (12) [32,33]:

$$R_G = \frac{1}{A} \cdot \frac{dm}{dt} = \frac{3\alpha}{\beta} \cdot \rho_{Sco} G = \frac{3\alpha}{\beta} \cdot \rho_{Sco} \frac{dL}{dt} \tag{12}$$

where A is the particle area (m^2), m is the mineral mass (kg), ρ_{Sco} is the scorodite density (3280 kg m^{-3}), and α and β are volume and shape factors. For octahedra, $6\alpha/\beta = 0.816$ [34]. From Equation (12), the linear growth rate can be expressed by Equation (13).

$$G = \frac{dL}{dt} = \frac{\beta}{3\alpha \cdot A \cdot \rho_{Sco}} \cdot \frac{dm_{Sco}}{dt} \tag{13}$$
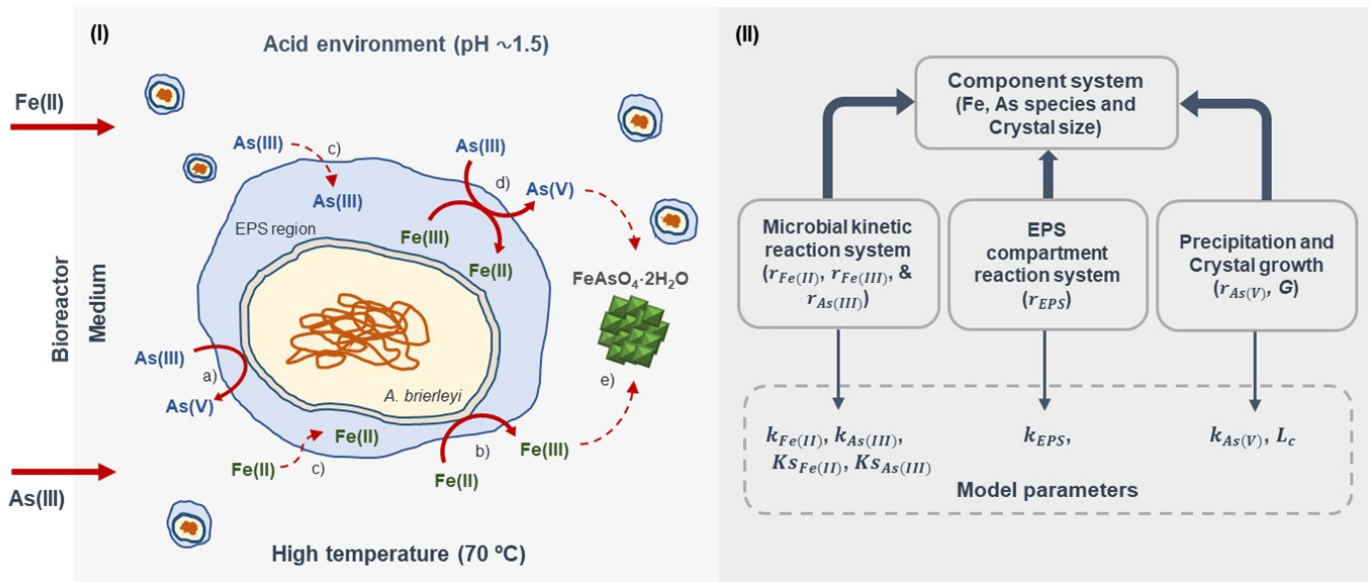

Figure 1. (**I**) Schematic representation of the possible phenomena involved in the bioscorodite formation [9]: (a) microbial As(III) oxidation, (b) microbial Fe(II) oxidation, (c) ions concentrated in the EPS region, (d) oxidation/reduction reactions in the EPS region, and (e) bioscorodite crystallization. (**II**) Modeling approach for modeling the simultaneous processes for bioscorodite formation.

The rate of change in scorodite mass related to As(V) precipitation in the solution is given by Equation (14),

$$\frac{dm_{Sco}}{dt} = M_{Sco} \cdot V \cdot \left(\frac{dAs(V)}{dt} \right) \cdot k_{As(V)} [Fe(III)][As(V)] \tag{14}$$

where m_{Sco} is the mass of bioscorodite (kg), M_{Sco} is the molecular weight of scorodite (0.230 kg mol^{-1}), V is the reaction volume (L), and dAs(V)/dt is the time derivative for arsenic precipitation (mmol L^{-1}). Then, from the equations of total mass (Equation (15)) and superficial area (Equation (16)), we obtain Equation (17).

$$W = n \cdot \rho_{Sco} \cdot \alpha \cdot L_c^3 \tag{15}$$

$$A = n \cdot \beta \cdot L_c^2 \tag{16}$$

$$\frac{\beta}{\alpha \cdot A} = \frac{L_c \cdot \rho_{Sco}}{W} \tag{17}$$

where W is the mass of crystals (kg), n is the number of crystals (dimensionless) and L_c is the characteristic crystal size (m). By replacing Equation (17) in Equation (13) and substituting in Equation (14), Equation (17) is obtained, which upon integration yields the crystal size (m) over time.

$$G = \frac{dL}{dt} = \frac{L_C \cdot M_{Sco} \cdot V}{3 \cdot W} k_{As(V)} [Fe(III)][As(V)] \tag{18}$$

2.2. Saturation Index of Bioscorodite

The saturation index (SI) is a parameter used to assess the formation of a mineral phase. Accordingly, three cases can occur in solution: (i) SI < 0, the aqueous phase is undersaturated, and the scorodite mineral can dissolve in the medium; (ii) SI = 0, the

aqueous phase is at equilibrium; and (iii) SI > 0, the aqueous phase is supersaturated, and chemical precipitation occurs. The SI of bioscorodite was calculated according to Equation (19) [35].

$$SI = \log_{10}\left(\frac{\left(a_{Fe(III)}\right)\left(a_{As(V)}\right)}{K_{sp,Sco}}\right) \quad (19)$$

where $a_{Fe(III)}$ and $a_{As(V)}$ are the ion activities of Fe(III) and As(V), respectively, and $K_{sp,Sco}$ is the solubility product constant of scorodite ($10^{-21.7}$) [36]. The chemical activities of Fe(III) and As(V) were calculated with Equations (20) and (21), using the pH values ($a_{H+} = 10^{-pH}$) and the total soluble concentrations of Fe(III) and As(V) (mM), respectively. For all cases, the proton concentration was assumed constant (pH = 1.5). The hydrolysis constants (K_i) for Fe(III) and As(V) are shown in Table 1.

$$a_{Fe(III)} = \frac{Fe(III)}{1 + \frac{K_{Fe,1}}{a_{H+}} + \frac{K_{Fe,1}K_{Fe,2}}{\left(a_{H+}\right)^2} + \frac{K_{Fe,1}K_{Fe,2}K_{Fe,3}}{\left(a_{H+}\right)^3} + \frac{K_{Fe,1}K_{Fe,2}K_{Fe,3}K_{Fe,4}}{\left(a_{H+}\right)^4}} \quad (20)$$

$$a_{As(V)} = \frac{As(V)}{1 + \frac{a_{H+}}{K_{As,3}} + \frac{\left(a_{H+}\right)^2}{K_{As,2}K_{As,3}} + \frac{\left(a_{H+}\right)^3}{K_{As,1}K_{As,2}K_{As,3}}} \quad (21)$$

Table 1. Hydrolysis constants for arsenate and ferric iron at 70 °C [37].

Chemical Specie	Reaction	Ki	pK
As(V)	$H_3AsO_4 \rightarrow H_2AsO_4^- + H^+$	$K_{As,1}$	2.27
	$H_2AsO_4^- \rightarrow HAsO_4^{2-} + H^+$	$K_{As,2}$	6.94
	$HAsO_4^{2-} \rightarrow AsO_4^{3-} + H^+$	$K_{As,3}$	11.51
Fe(III)	$Fe^{3+} + H_2O \rightarrow Fe(OH)^{2+} + H^+$	$K_{Fe,1}$	2.18
	$Fe(OH)^{2+} + H_2O \rightarrow Fe(OH)_2^+ + H^+$	$K_{Fe,2}$	3.47
	$Fe(OH)_2^+ + H_2O \rightarrow Fe(OH)_3 + H^+$	$K_{Fe,3}$	6.31
	$Fe(OH)_3 + H_2O \rightarrow Fe(OH)_4^- + H^+$	$K_{Fe,4}$	9.57

2.3. Model-Data Fitting Approach

The experimental data sets employed for model fitting describe time-varying concentrations of Fe(II), Fe(III), As(III) and As(V) obtained from two different studies (details can be found in Section 3). The fit of the nonlinear model to the experimental data represents a complex optimization problem, which was addressed by the Levenberg–Marquardt algorithm for solving the nonlinear least squares problem. The mathematical equations composing the model were programmed in the Model-Maker® version 3.0.3 (Cherwell Scientific Publishing Ltd., Oxford, UK) software, employing a block diagram. The parameter estimation toolbox was used to find the minimum value of the objective function (F_{obj}, residual sum of squares) and the parameter set that provides the best fit. The fourth order Runge–Kutta algorithm was set in the software to solve the differential equations of the model with a constant step size of 0.1. The optimization stop criterion was a relative sum of the square change of 1×10^{-3}. Furthermore, individual determination coefficients (R^2) and residuals were obtained from linear regression, which were then analyzed to evaluate the model predictive capacity.

2.4. Software and Simulations

Simulink® ((Nettik, MA, USA) was used as a simulation platform to analyze the dynamic behavior of the bioscorodite crystallization process under different scenarios. Simulink® works within the MATLAB® (R2017a, (Nettik, MA, USA) software and simulates the process dynamics in terms of a block diagram with interconnections and sends the results to MATLAB for further data processing. The variable-step ode23s solver was used

to solve the ordinary differential equations of the model. All numerical simulations were performed on a PC equipped with an Intel® Core© i5 processor and 8 GB of RAM.

2.5. Global Sensitivity Analysis

One of the main functions of global sensitivity analysis (GSA) in modeling tasks is to identify target parameters for further theoretical and experimental exploration [38]. A GSA was conducted to identify critical parameters in the parameter space that strongly influence the model outputs and to determine the parameters whose influence is essentially negligible [39]. The GSA was performed as follows: Monte Carlo simulations were programmed in Simulink® (Nettik, MA, USA), generating 100 random samples per parameter which follow a normal distribution ($1/\sigma\sqrt{2\pi}e^{-\frac{1}{2}(\frac{X-\mu}{\sigma})^2}$) where μ and σ are the mean and standard deviation, respectively. Then, the signal matching time-domain design requirement was defined as a cost function in the software, which is then evaluated for each generated combination of parameters by solving the kinetic model. Finally, standardized linear regression coefficients are generated to analyze the relationship between the parameters and the design requirement (model evaluation).

2.6. Statistical Analysis

The confidence intervals (C.I., 95%) of the adjusted parameters were determined in the Model-Maker® (Cherwell Scientific Publishing Ltd., Oxford, UK) software. A statistical treatment was conducted for the fitted parameters, which were analyzed with a one-way analysis of variance (ANOVA) using Microsoft Excel with an $\alpha = 0.05$.

3. The Experiments

The crystallization process of biogenic scorodite has been studied due to its promising results for the immobilization of arsenic from metallurgical wastewater [25,40,41]. The crystallization of this mineral is biologically induced, where Fe(II) oxidation is first carried out by extremophilic microorganisms, and As(V) is then fed to the bioreactor where As(V) precipitates as scorodite. The above process scheme was proposed by González-Contreras et al. [32]. However, since arsenic is mainly found in its trivalent form in metallurgical wastewater, Okibe et al. [9] proposed a one-step process to remove arsenic, initiating the process with the simultaneous oxidation of Fe(II) and As(III) by Acidianus brierleyi to obtain Fe(III) and As(V), which react and precipitate as bioscorodite. It is important to note that these processes occur in the same bioreactor.

Arsenic precipitation in the form of scorodite is usually evaluated under extremophilic culture conditions (high temperature and acidic pH) to provide an optimal environment to oxidize microbes and promote scorodite formation. Selected experimental campaigns from Okibe et al. [27] and Tanaka et al. [42], where scorodite formation was observed, were used for parameter estimation and model validation. Table 2 shows the main characteristics of the experiments. In both studies, the experiments were performed using Acidianus brierleyi to oxidize iron and arsenic, using 1×10^7 cells mL^{-1} as the initial cell concentration and an initial pH of 1.5 for all systems. Okibe et al. [27] performed their experiments using different initial concentrations of Fe(II) and As(III) but maintained an Fe/As molar ratio of 1.4. On the other hand, Tanaka et al. [42] employed an initial Fe/As ratio of 1.4 using seeding material (scorodite). All campaigns were carried out using a defined growth medium supplemented with yeast extract (0.01–0.02 w/v %) in 500 mL shake flasks with 200 mL working volume, using a constant temperature and agitation of 70 °C and 100 rpm, respectively. Samples were taken periodically to measure cell density, pH, and concentrations of As(III), As(V), Fe(II), and total Fe. For further technical aspects on experimental setup, culture, medium composition or solid analysis, the reader is referred to the works of Okibe et al. [27] and Tanaka et al. [42].

Table 2. Characteristics of the experiments employed for model evaluation.

System Name	Inoculum (cells mL^{-1})	Fe(II)$_0$ (mM)	As(III)$_0$ (mM)	Fe/As Molar Ratio ($-$)	Yeast Extract (%, *w/v*)	Seeding Material
S-1 [a]	1×10^7	6.58	4.7	1.4	0.02	Scorodite
S-2 [b]	1×10^7	9	6.5	1.4	0.01	-
S-3 [b]	1×10^7	18	13	1.4	0.01	-
S-4 [b]	1×10^8	18	13	1.4	0.01	-

Experimental data from: [a] Tanaka et al. [35], [b] Okibe et al. [23].

4. Results and Discussion

4.1. Sensitivity Analysis

The sensitivity of the parameters was strongly influenced by the initial conditions used for the experimentation, which were used to perform the GSA. Variations in sensitivity can be explained through the phenomenology of the process, as the contribution in ion oxidation, either by microbial oxidation or by the EPS region, can change. To know the sensitivity under different culture conditions, GSA was performed under three different scenarios (Experiments S-1, S-2 and S-3) using the initial conditions shown in Table 2 and considering a cell concentration of 1×10^7 cells mL^{-1} which, using an average cell weight of 1 pg, was converted to 0.01 gbiomass L^{-1}. Figure 2 shows the sensitivity indices of the parameters $k_{Fe(II)}$, $k_{As(III)}$, k_{EPS}, $k_{As(V)}$, $Ks_{Fe(II)}$ and $Ks_{As(III)}$ for the variables Fe(II), Fe(III), As(III) and As(V). Commonly, parameters with low sensitivity indexes present a minor effect on model predictions, while parameters with high sensitivity indexes present a strong influence on model results, thus requiring higher certainty to improve model robustness [38,43]. From the GSA of S-2, it can be observed that the most sensitive parameters vary from one variable to another. Note that the Fe(II) and Fe(III) variables are strongly influenced by the oxidation rate constant ($k_{Fe(II)}$) and the iron affinity constant ($Ks_{Fe(II)}$). In addition, the variables As(III) and As(V) are mainly influenced by the arsenite affinity constant ($Ks_{As(III)}$) and the arsenite oxidation rate constant ($k_{As(III)}$). In addition, these sensitive parameters are followed by the oxidation rate constant for the EPS compartment (k_{EPS}). The high degree of sensitivity of the above parameters indicates that they were adequate and sufficient in the sense of making a simple but robust mathematical model capable of accurately predicting the oxidation processes (as detailed in Section 4.2), according to the proposed equations and phenomenological scheme. On the other hand, these facts provide a basis for linking the level of sensitivity to the contribution of the enzymatic activity and the EPS region in the oxidation process (Equation (2)). From the overall GSA (all experiments), in general terms, the oxidation rate constants ($k_{Fe(II)}$ and $k_{As(III)}$) and the precipitation rate constant ($k_{As(V)}$) were the parameters with the highest sensitivity indexes, and we noticed that these parameters have a relevant role in the proper performance of all the biosystem variables. Therefore, these parameters were prioritized in the model calibration for the three scenarios. These observations are in line with experimental observations which indicate that bioscorodite crystallization is controlled by Fe(II) oxidation [6,24,37]. Furthermore, these results indicate that the As(III) oxidation step can also be considered as an additional bottleneck of the process, and since trivalent arsenic is mostly found in metallurgical wastewater, there is a special interest in improving this step. Furthermore, the effect of ion concentration on As(V) precipitation seems to be a relevant factor to take into account in the process design, since it can be seen that the sensitivity index of the precipitation rate constant ($k_{As(V)}$) increases dramatically at high ion concentrations. Figure 2 also shows that the higher the ion concentration, the higher the sensitivity of $k_{As(III)}$. Furthermore, it was observed that the sensitivity of k_{EPS} for the variable As(III) increases as the ion concentrations increase (from S-1 to S-3). Conversely, for the Fe(II) variable, the sensitivity of k_{EPS} decreases as Fe(II) concentrations increase. These changes can be explained by differences in the concentration of yeast extract used in the experiments (0.01 to 0.02 % *w/w*), since this substrate is closely related to the formation

of the microbial EPS matrix [10,27]. Moreover, variations in this parameter can be related to As(III) concentration, since it depends linearly (R^2 = 0.98) on this variable, which leads us to think that high ion concentrations promote the development of the EPS region to protect cells from As(III) and facilitate its oxidation to As(V) [27,44]. In turn, these changes may be related to the degree of contribution of the redox reactions taking place in the EPS compartment, i.e., at low ion concentrations the EPS reactions contribute largely to the formation of Fe(II) and As(V) ions (see Equation (2)), whereas at higher ion concentrations the predominance of enzymatic over ionic oxidation in the EPS region may be noticeable. The evaluation of a wider range of yeast extract concentrations in the oxidation process should be performed in the future using experimental and numerical tools.
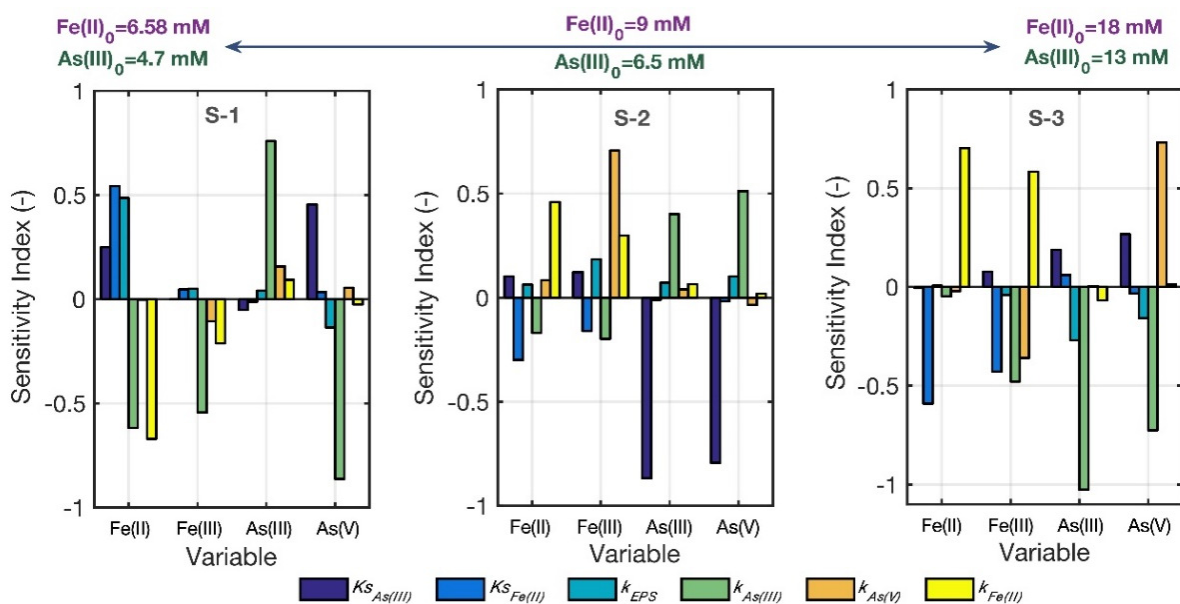

Figure 2. Sensitivity indices for the Fe(II), Fe(III), As(III) and As(V) variables from the experiments S-1, S-2 and S-3.

4.2. Parameter Fitting Results and Statistics

Parametric identification was performed in Model-Maker® (Cherwell Scientific Publishing Ltd., Oxford, UK) software by fitting the mathematical model to different experimental data sets. The model parameter set consists of six kinetic constants, i.e., $k_{Fe(II)}$, $k_{As(III)}$, k_{EPS}, $k_{As(V)}$, $Ks_{Fe(II)}$, and $Ks_{As(III)}$. The characteristic crystal size (L_c) was fitted empirically. The first set of parameters was obtained by fitting the model to the experimental data set S-2, considering the initial conditions $Fe(II)_0$ = 9 mM, $Fe(III)_0$ = 0 mM, $As(III)_0$ = 6.5 mM, and $As(V)_0$ = 0 mM. All experiments were performed considering a cell concentration of 1×10^7 cells mL^{-1} (0.01 $g_{biomass}$ L^{-1}) and assuming a constant pH of 1.5. From this estimation, the parameters $Ks_{Fe(II)}$ and $Ks_{As(III)}$ were kept constant when evaluating the model with experimental data sets S-1 and S-3. This procedure was performed considering the high sensitivity of these parameters and considering that the same microorganism (*A. brierleyi*) is used for all experiments. Note that $Ks_{Fe(II)}$ was similar to that observed for *A. brierleyi* in a scorodite crystallization system reported by Tec-Caamal et al. [23] (31.16 mM). The remaining parameters, $k_{Fe(II)}$, $k_{As(III)}$, and $k_{As(V)}$, were adjusted for each campaign, considering that differences in concentrations may lead to changes in the metabolic capacity for iron and arsenic oxidation, on which arsenic precipitation depends. In addition, due to the variable sensitivity of k_{EPS} as ion concentrations change, this parameter was fitted for all experiments (from S-1 to S-3). Table 3 presents the model parameter values with their 95% confidence interval. The observed parametric uncertainty for some parameter values can be explained mainly by the fact that samples must be obtained from shake flasks and analyzed offline with finite precision, which is coupled with the nonlinear nature of biological

systems [43]. Table 3 also shows that for all experiments there were statistically significant differences between the fitted parameters $k_{Fe(II)}$, $k_{As(III)}$, k_{EPS}, and $k_{As(V)}$, indicating that the initial concentration of Fe(II) and As(III) exerts a strong influence on the microbial ability to oxidize ions and precipitate arsenic. R^2 coefficients, residual analysis and *p*-values were used as criteria to evaluate the model's capability to predict Fe(II) and As(III) oxidation, As(V) precipitation, and scorodite crystallization under different scenarios. Overall, R^2 coefficients greater than 0.95 (with *p*-values <0.001) for all experiments suggest that there are no statistically significant differences between the experimental and predicted data. Furthermore, a randomly distributed trend of the residuals for all variables indicates, in global terms, the good predictive ability of the model [45].

Table 3. Parameter values and their confidence intervals (95%) for the experiments from Table 2.

Parameters			Experiments		
Symbol	Description	Units	S-1	S-2	S-3
$k_{As(III)}$ [c]	Arsenite oxidation rate constant	mM (d $g_{biomass}$)$^{-1}$	501.38 ± 3.36	395.9 ± 65.53	109.17 ± 14.14
$k_{As(V)}$ [c]	Arsenate precipitation constant	L (mM d)$^{-1}$	0.004 ± 0.0008	0.006 ± 0.001	0.018 ± 0.002
$k_{Fe(II)}$ [c]	Ferrous iron oxidation rate constant	mM (d $g_{biomass}$)$^{-1}$	$38{,}577.03 \pm 8744.07$	4553.4 ± 1174.79	3896.2 ± 310.83
k_{EPS} [a]	Arsenite oxidation rate constant for the EPS region	mM^2 d^{-1}	$0.0002856 \pm 1 \times 10^{-6}$	0.0012 ± 0.03	0.0154 ± 0.009
$Ks_{As(III)}$ [a]	Affinity constant for arsenite	mM	1.82 ± 0.51	1.82 ± 0.51	1.82 ± 0.51
$Ks_{Fe(II)}$ [a]	Affinity constant for ferrous iron	mM	36.67 ± 3.42	36.67 ± 3.42	36.67 ± 3.42
L_c [b]	Characteristic crystal size	μm	0.305	0.305	0.32
Global R^2	Global determination coefficient	Dimensionless	0.96	0.95	0.98

[a] Parameters initially determined by fitting the model to experimental data set S-3, which were then kept constant for the experiments S-1 and S-2. [b] No confidence interval available due to empirical estimation. [c] Parameter with statistically significant difference between treatments (H$_1$: alternative hypothesis).

4.3. Mathematical Model Validation

The predictive ability of the proposed mathematical model was evaluated under three different scenarios in batch systems, considering the initial conditions reported by Okibe et al. [27] and Tanaka et al. [42], where the initial Fe(II) concentration varied in the range of 6.5–18 mM and the initial As(III) concentration varied in the range of 4.6–13 mM, resulting in initial Fe(II)/As(III) molar ratios of 1.4 in all experiments (see Table 2). Figure 3 shows the performance of the mathematical model versus experimental data for Fe(II) and As(III) oxidation, Fe(III) generation, and As(V) precipitation, where it can be seen that, in general terms, the model predictions follow the experimental trend. Individual R^2 coefficients between 0.79 and 0.99 (with *p*-values < 0.001) and modeling efficiency indices for all state variables (Table S1, Supplementary Materials) show the adequate performance of the proposed mathematical structure and help to reinforce the validity of the proposed parameter values. In the system studied, *Acidianus brierleyi* is expected to oxidize Fe(II) and As(III) ions by two pathways occurring simultaneously, i.e., enzymatically and in the EPS region. Then, Fe(III) and As(V) react to form scorodite. The EPS compartment can be understood as a region where ions are concentrated by complexation, increasing the contact between ions for redox reactions, thus enhancing the oxidation process. It should be noted that both oxidation mechanisms (enzymatic at the cellular level and by the EPS matrix) can be considered as biological processes, since *A. brierleyi* oxidizes Fe(II) and As(III) enzymatically, but also by the exopolysaccharides produced by itself [11–13]. The model built on the basis of both mechanisms was able to accurately describe the overall oxidation of Fe(II) and As(III) and the precipitation of As(V) (Figure 3). In addition, the model allows predicting saturation index trajectories over time, which were comparable with other trajectories found in the literature under comparable operating conditions in batch reactors [16,25]. Simulated SI values (at constant pH = 1.5) showed that the values were never in equilibrium (never zero), indicating the precipitation of scorodite in solution, reaching a maximum value at day 2 (Figure 3D). In addition, Log IAP values reach values

higher than the K_{sp} value for scorodite ($10^{-21.7}$) during the entire culture time [16,23,25] (Figure S1, Supplementary Materials), indicating that the solution was supersaturated in that period. Furthermore, by coupling the crystal growth model developed by Gonzalez-Contreras et al. [32] and the proposed model for oxidation/precipitation, it was possible to predict the crystal size of 1 µm from the experimental sets S-2 and S-3 [27], and 71 µm for the estimate of Tanaka et al. [42] (S-1) (see Figure S2, Supplementary Materials). A larger crystal size was observed in the latter campaign, as this experiment was conducted with an initial scorodite seed load with an approximate size of 70 µm [35]. The characteristic crystal size (L_c, Equation (18)) for experiments S-2 and S-3 was adjusted to 0.305 µm, and to 0.32 µm for S-1.
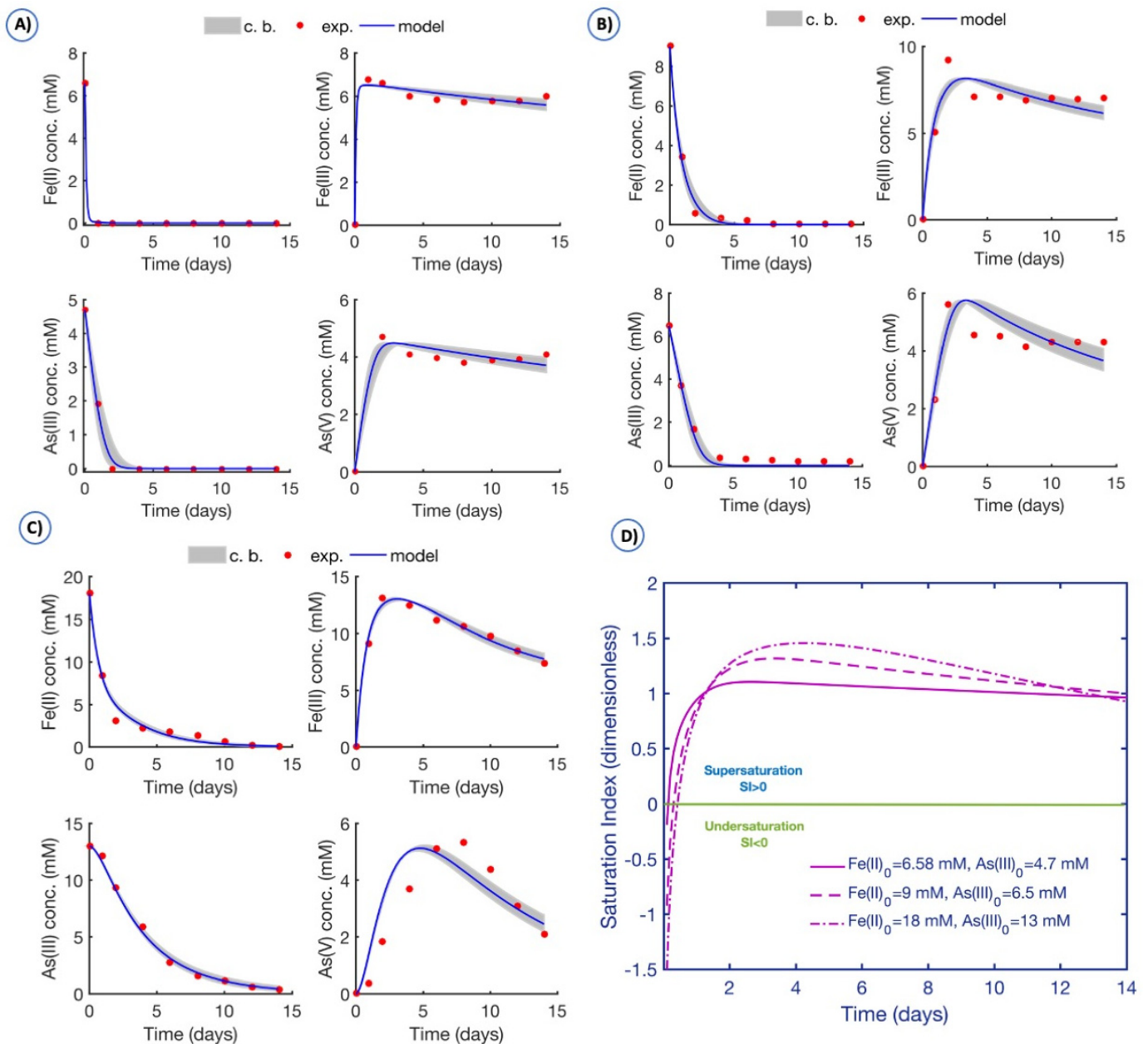

Figure 3. Model evaluation and confidence bands for different data sets performed on Fe(II)/As(III) = 1.4: (**A**) S-1, experiment with Fe(II)$_0$ = 6.58 mM and As(III)$_0$ = 4.7 mM; (**B**) S-2, experiment, with Fe(II)$_0$ = 9 mM and As(III)0 = 6.5 mM; (**C**) S-3, experiment with Fe(II)$_0$ = 18 mM and As(III)$_0$ = 13 mM. (**D**) Saturation index simulation for all experiments. Experimental data source: Okibe et al. [27] and Tanaka et al. [42].

The mathematical model was also evaluated with an additional experiment (S-4, Table 2) in which a higher cell concentration (1×10^8 cells mL^{-1}) was used. In this campaign, the complete oxidation of As(III) was observed on day 3, and As(V) was fully precipitated on day 8, which was also predicted by the proposed model by empirically fitting the parameters k_{EPS} (0.0378 mM^2 d^{-1}) and $k_{As(V)}$ (0.096 L mM^{-1} d^{-1}) (Figure S3, Supplementary Materials). The increased k_{EPS} value for this condition may be related to a higher amount of exopolysaccharide produced by microbes, which is possibly due a higher initial cell concentration. This can be noted by comparing the k_{EPS} value for a lower cell concentration, such as k_{EPS} = 0.0154 mM^2 d^{-1} for the cell concentration of 1×10^7 cells mL^{-1} (Table 3). The experimental crystal size was approximately 1 μm, which was also simulated by the model using a L_c value of 0.375 μm (Figure S3, Supplementary Materials). From these observations, the model was found to have a robust ability to simulate the bioprocess under different scenarios.

4.4. Model-Based Analysis of Controlling Factors on the Bioscorodite Crystallization Process

Model-based bioprocess analysis can provide valuable information of the system dynamics under different scenarios through simulation analysis. The objective of this section is to employ the mathematical model to explore the effect of different factors on oxidation rates, percent arsenic removal, and bioscorodite crystal size. Here, the effect of cell concentration, initial Fe(II) and As(III) concentrations, and kinetic parameters related to microbial oxidation capacity and oxidation through redox reactions taking place in the EPS compartment formed by the microbes are analyzed. For this purpose, simulations were performed using the model described in Section 2, which was implemented in a block diagram in Simulink® (Nettik, MA, USA). The simulations were performed assuming a constant bioreactor temperature (70 °C) and pH (at 1.5) and considering a batch culture time of 14 days. The ranges of the variables analyzed were based on literature data.

4.4.1. Cell Concentration

In the process, microbial cells are responsible for oxidizing Fe(II) and As(III) to Fe(III) and As(V), respectively. However, the low growth rate and low cell yield of thermoacidophilic microbes has been described as the limiting step in the immobilization of arsenic as a bioscorodite [34]. Since the concentration of cells in the reactor exerts an effect on Fe(II) and As(III) oxidation rates, which in turn affects the bioscorodite crystallization process, it is interesting to analyze the effect of this factor on the overall process. As explained in Section 2, the model is built based on the assumption of a constant cell concentration, which is well supported by experimental observations [27,28,46]. Model simulations were performed using the initial conditions of experiment S-3 and the following cell concentrations (C_{bio}) 1×10^6, 2.5×10^6, 1×10^7, and 1×10^8 cells mL^{-1}. Simulations were performed considering the absence of seeding material. The effect of the cell concentration on Fe(II) and As(III) oxidation and As(V) precipitation is depicted in Figure 4A, where it can be observed that the percentage of oxidation of Fe(II) and As(III) increases as the cell concentration increases, reaching 100% oxidation at cell concentrations of 1×10^7 and 1×10^8 cells mL^{-1}, which are obtained mainly by the availability of a greater number of cells for oxidation, allowing the complete oxidation of both ions in less time. It can also be observed that the biomass concentration has an influence on As(V) removal. The higher the cell concentration, the higher the precipitation percentage, i.e., from 19 to 87% for the increasing range of biomass concentration. These results are in line with the experimental observations of Okibe et al. [27], who indicate that high cell concentrations lead to precipitate As(V) in less time. Moreover, Figure 4C shows that cell concentration also impacts the crystal size. In the evaluated range of cell concentration, the crystal size increases from 0.96 to 1 μm, which is related to changes in the percentage of As(V) precipitated. In addition, the changes in crystal size are related to the SI behavior (Figure 4D), where it can be noticed that supersaturation (SI > 0) is reached in a shorter time as cell concentration increases. These results agree with the numerical observations of Tec-Caamal et al. [23].
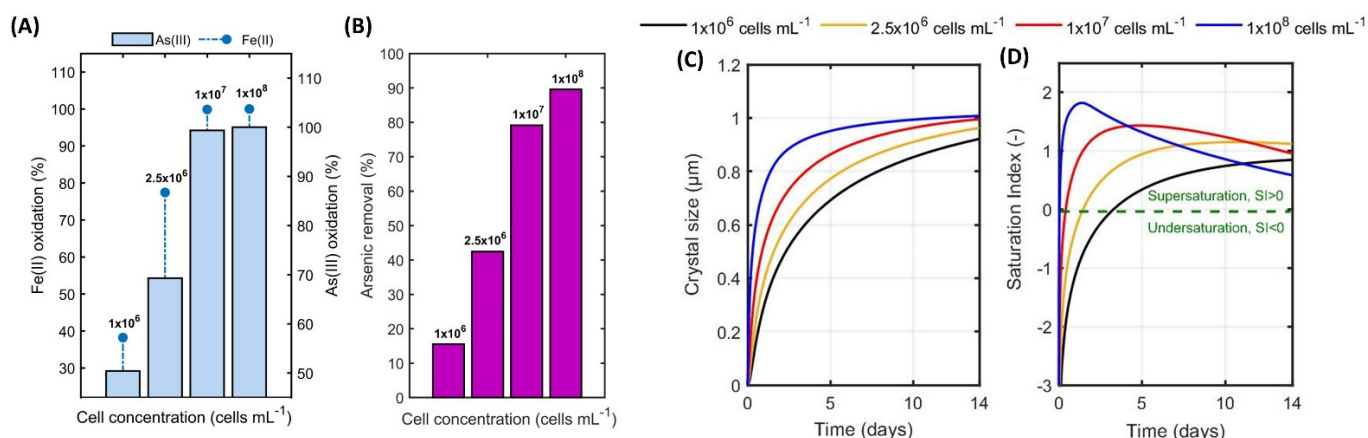
Figure 4. Model-based evaluation of the cell concentration of the process (14-day culture): (**A**) Fe(II) and As(III) oxidation; (**B**) arsenic removal; (**C**) crystal size; (**D**) saturation index of bioscorodite.

4.4.2. Fe(II) and As(III) Concentrations at Fe/As = 1.4

The Fe(II) concentration strongly affects the crystallization process of bioscorodite. This fact has been observed in the process scheme proposed by González-Contreras et al. [14], where Fe(II) is microbially oxidized to Fe(III), and arsenic is introduced into the reactor in its pentavalent form. In the process configuration analyzed in this study, arsenic is in its trivalent form, and needs to be oxidized prior to precipitation, so it is important to study the effect of the concentration of both ions on the overall process [47].

The relevance of characterizing this effect is due to the fact that the oxidation of both ions occurs simultaneously but can take place at different rates (see Figure 3C). Experiments with *A. brierleyi* cultures showed that the initial Fe(II)/As(III) molar ratio is a relevant factor in achieving high arsenic removal efficiencies, with an optimum value of 1.4 being found to achieve 98–99% arsenic removal [37]. Note that this value is close to the stoichiometric ratio shown in Equation (4), where it is observed that 1-mol Fe(II) is needed to precipitate 1-mol arsenic. This value also shows that low amounts of iron are needed for arsenic precipitation. Furthermore, Fe/As > 2 can lead to the formation of undesirable secondary minerals, as indicated by Okibe et al. [27]. From this, all simulations were performed using different initial ion concentrations, but keeping Fe(II)/As(III) = 1.4, and considering the absence of foreign seeds. The set of adjusted parameters and initial conditions from experiment S-2 were used for the simulations. The upper and lower limits of Fe(II) and As(III) concentration were chosen according to the literature where no microbial inhibition was observed, i.e., 8.4–28 mM for Fe(II) and 6–20 mM for As(III) [14,37,42]. Figure 5 illustrates the effect of the initial concentrations of Fe(II) and As(III) on the overall process, where it can be observed that 100 % oxidation is reached for Fe(II) and As(III). Moreover, it can be noted that As(V) precipitation increases as the ion concentration increases, reaching a maximal percentage of precipitation of 71 % (Figure 5B).

This process behavior is consistent with the experimental observation of Tanaka et al. [37], who noticed that by maintaining an initial Fe/As molar ratio of 1.4, but increasing the initial As(III) concentration from 4.7 to 13 mM, As(V) removal can increase from 15 to 99 %. Theoretical results also agree with numerical simulations of Tec-Caamal et al. [23]. This figure shows that Fe(II) oxidation is oxidized to the same extent as that of arsenic. Moreover, it is important to note that the cell concentration used for simulations was adequate, since it allowed for complete ion oxidation in a 14-day batch culture. The remaining As(V) and Fe(III) ions in the aqueous phase are expected to precipitate in the next days, as confirmed with numerical simulations with a culture time of 25 days. Figure 5B show that the crystal size increases as the As(V) precipitation increases, reaching a maximal size of 1.08 μm. The saturation index for the different initial conditions shows that the solution becomes supersaturated in less time as the initial ion concentration increases. Vega-Hernandez et al. [25]

suggest that supersaturation can be controlled by Fe(II) oxidation. If SI values are less than 1.5, few nuclei can be expected to form, resulting in larger particles. In general, it was observed that under the simulated conditions tested, the process can deal with high arsenic concentrations, but the Fe(II)/As(III) molar ratio should be kept at 1.4, since Fe(II) and As(III) are rapidly oxidized in the first few days.
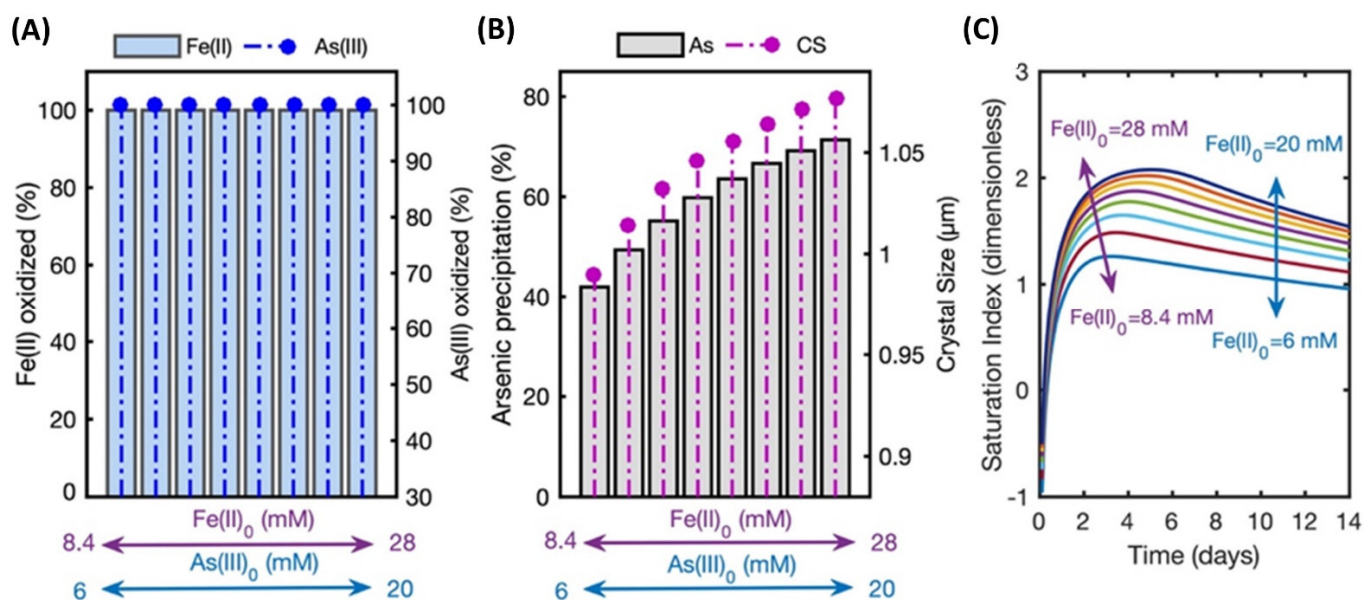

Figure 5. Effect of initial Fe(II) and As(III) concentrations on the scorodite crystallization process, maintaining an initial Fe(II)/As(III) molar ratio of 1.4 (**A**–**C**).

4.4.3. Analysis of k_{EPS} on the Overall Process

The EPS compartment is a relevant factor in explaining the ion oxidation and precipitation of As(V) as scorodite, which was considered in the proposed model structure. In this section, the effect of this factor is analyzed by simulation in terms of the oxidation rate constant for the EPS region, k_{EPS}. As shown in Table 3, k_{EPS} values change from one culture condition to another, which is mainly related to variations in the yeast extract (used as a supplementary substrate) and cell concentration. Both factors lead to the formation of the EPS matrix, thus enhancing oxidation rates [14,27,42]. Since k_{EPS} is susceptible to changes in culture, we analyzed the effect of k_{EPS} variations on the overall process. For this purpose, we considered the upper and lower limits obtained in the model fitting procedure (2.85×10^{-4}–0.0154 mM^2 d^{-1}, see Table 3) and the initial conditions of experiment S-3. The simulation results show that the higher the value of k_{EPS}, the higher the maximum oxidation percentages of Fe(II) and As(III) (obtained at the inflection point), which increase linearly (Figure 6A,B). The simulation also showed that k_{EPS} changes do not exert a strong influence on the Fe(II) oxidation percentage, which is almost complete at day 14, but significant variations were observed for As(III) oxidation ranging from 88.6 to 99% for the increasing range of k_{EPS}. It can also be observed that total arsenic removed increases from 64 to 79% for all scenarios. These results are consistent with the sensitivity analysis in Section 4.1, where it was observed that the As(III) variable is very sensitive to k_{EPS} variation (in particular at high concentrations), but the Fe(II) variable is not. These results also suggest that by varying the culture conditions (particularly ion and yeast concentrations), As(V) generation by the EPS region can be promoted (see Equation (2) and Figure 1). On the other hand, the maximum saturation index was about 1.43 for all simulated conditions, indicating that bioscorodite minerals formed in the aqueous phase, reaching SI > 0 after 0.5 days of culture for all cases [35]. Furthermore, as expected, k_{EPS} variations also affected crystal size, finding values between 0.96 and 1 μm for all conditions tested. Since k_{EPS} is susceptible to change depending on environmental conditions, further studies on yeast

extract and ion concentrations on arsenic oxidation and precipitation capacity should be performed in the future [47].
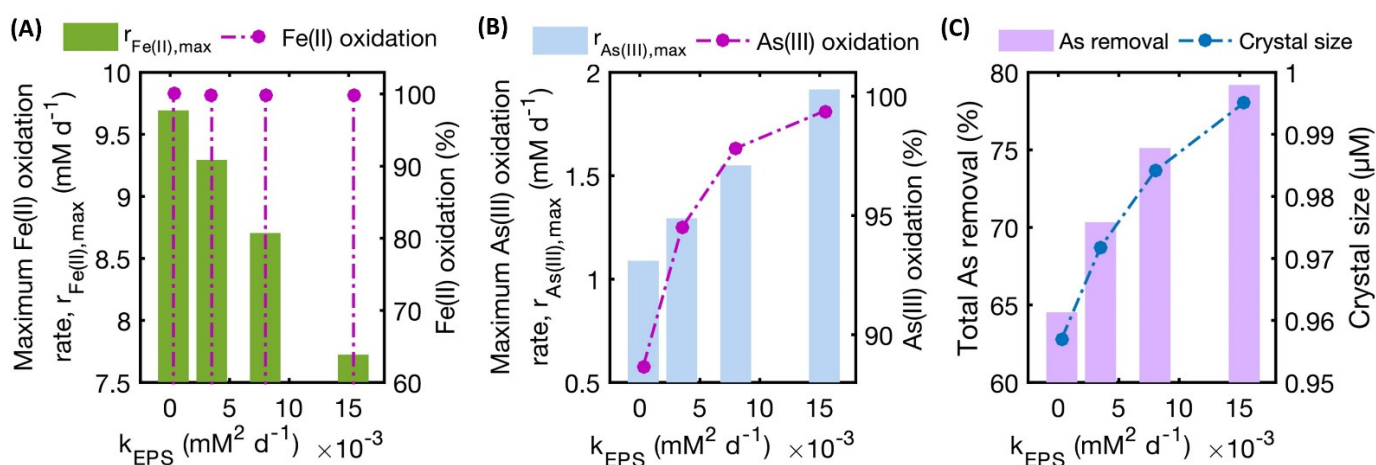

Figure 6. Effect of the oxidation rate constant for the EPS compartment (k_{EPS}) on the overall process, evaluated at 14-day culture operation (**A–C**).

4.4.4. Effect of Oxidation Rate Constants, $k_{Fe(II)}$ and $k_{As(III)}$

Microbial oxidation of Fe(II) and As(III) occurs simultaneously with oxidation in the EPS region, so it is interesting to analyze the oxidation capacity of *A. brierleyi* separately by evaluating the oxidation rate constants $k_{Fe(II)}$ and $k_{As(III)}$. Moreover, these parameters are influenced by the culture conditions, such as temperature, agitation, substrate availability, microorganism, and bioreactor configuration [14,28,48,49]. Furthermore, from Section 4.1, it can be observed that these constants are among the most sensitive parameters. Since variations in the parameters $k_{Fe(II)}$ and $k_{As(III)}$ are of importance in the process, a series of simulations were performed to evaluate their effect on the process performance, using parameter values within the ranges observed in the model fit (Table 3). The initial conditions from Experiment S-3 (Table 2) were used as initial conditions for the numerical runs. Figure 7 shows the simulations of As(III) and Fe(II) oxidation, As(V) precipitation, and crystal size as a function of $k_{Fe(II)}$ and $k_{As(III)}$ when *A. brierleyi* was grown for 2, 8, and 14 days. For all the indicated times, the simulated results revealed that As(III) oxidation is enhanced at high $k_{As(III)}$ and low $k_{Fe(II)}$. The same behavior is observed for crystal size, where crystals of 1.01 μm (maximum) are observed for the same conditions (Figure 7B) obtained at low $k_{As(III)}$ and high $k_{Fe(II)}$. This fact is explained by the slow oxidation of iron that allows controlling the supersaturation to levels that promote the formation of few nuclei, leading to the formation of larger crystals [6,25]. These results are supported by Figure S4 (Supplementary Materials), where it can be observed that Fe(II) oxidation is almost complete at day 2 for most $k_{Fe(II)}$ and $k_{As(III)}$ values, except for low $k_{Fe(II)}$ values (3.89×10^3–11.60×10^3, Figure S4), indicating that Fe(II) oxidation is less limited than that of As(III), thus noticing that As(III) oxidation as a process step that needs to be improved. However, Fe(II) oxidation may also be regulated, as oxidation controls the saturation index, which in turn influences the crystal size of bioscorodite. Further studies should be conducted in the future to analyze the effect of culture conditions on the ability of microbes to oxidize Fe(II) and As(III) (in terms of oxidation rate constants) in order to optimize the bioprocess.
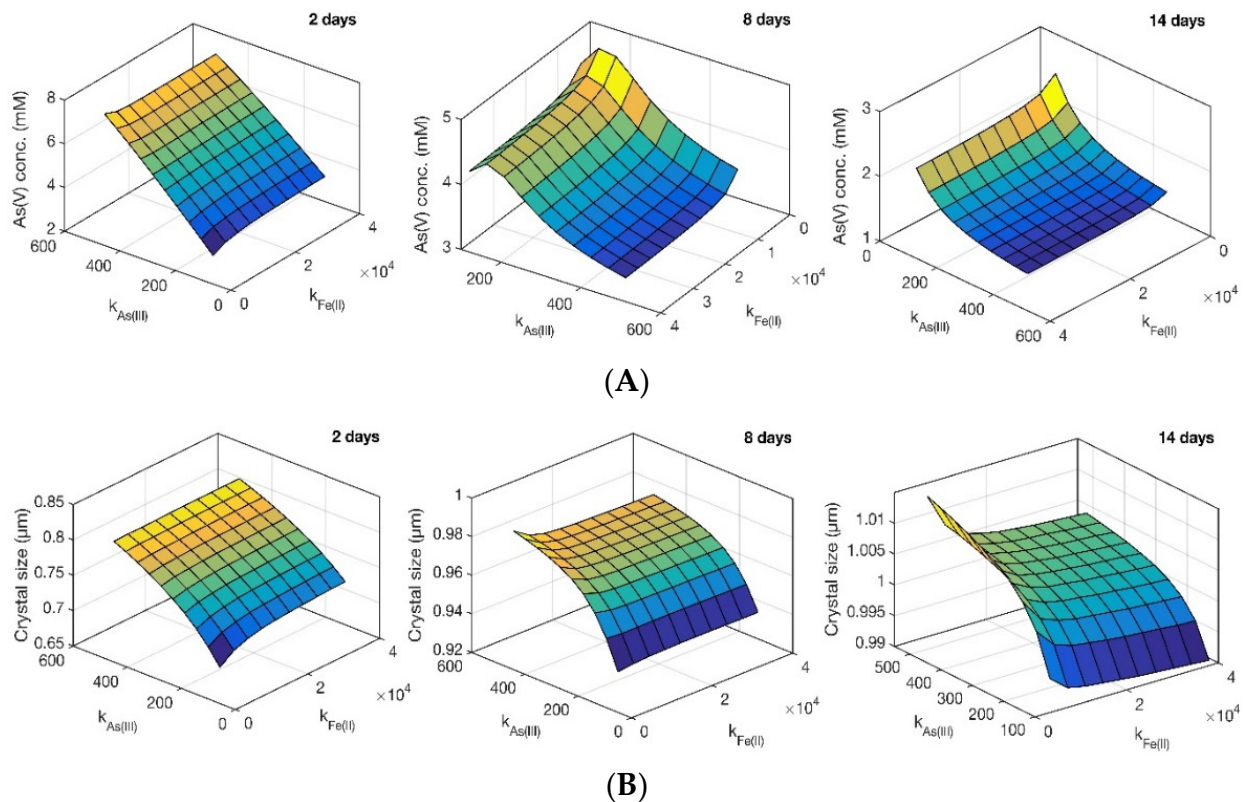
(A)

(B)

Figure 7. Effect of the oxidation rate constants, $k_{Fe(II)}$ and $k_{As(III)}$ (mM d^{-1} g$_{biomass}$$^{-1}$) on As(V) precipitation (**A**) and crystal size (**B**) at different culture times.

5. Conclusions

In this study, we propose a kinetic model to analyze the simultaneous processes involved in bioscorodite crystallization, considering Fe(II) and As(III) biooxidation by *Acidianus brierleyi* and the EPS matrix, As(V) crystallization, and crystal growth. Our approach is one of the first to provide a broad kinetic view of bioscorodite crystallization involving the synergistic effect of ion oxidation by the microbial pathway and by the EPS region. Our results indicate that the parameters $k_{Fe(II)}$, $k_{As(III)}$, and $k_{As(V)}$ were the most sensitive, indicating that these play a very important role in model prediction. The analysis of the factors controlling the process showed that high cell concentration can enhance As(V) precipitation up to 87% for 1×10^8 cells mL^{-1}. The initial ion concentration (Fe(II) and As(III)) was identified as a key factor in scorodite formation. It was found that by maintaining Fe/As = 1.4, and increasing the Fe(II) and As(III) concentrations, an increase in As(V) precipitation percentages is obtained (from 42% to 71%). Furthermore, the EPS region was found to be a relevant aspect in the overall process since changes in the medium composition can modify its value. Simulated results showed that an increase from 2.85×10^{-4} to 1.54×10^{-2} mM^2 d^{-1} can increase As(V) precipitation by 15 %. Furthermore, an evaluation of the oxidation rate constants indicated that high $k_{As(III)}$ and low $k_{Fe(II)}$ allow crystal sizes of about 1.01 µm at most for the evaluated biosystem. Due to the adequate predictive capability of the model, it can be used as a tool to propose reactor operation strategies, reactor design elements, optimization approaches, scale-up, and process control for the crystallization of biogenic scorodite in reactors under extremophilic conditions.

References

1. Chatterjee, D.; Adak, S.; Banerjee, N.; Bhattacharjee, P.; Bandyopadhyay, A.K.; Giri, A.K. Evaluation of health effects, genetic damage and telomere length in children exposed to arsenic in West Bengal, India. *Mutat. Res. Genet. Toxicol. Environ. Mutagen.* **2018**, *836*, 82–88. [CrossRef] [PubMed]
2. WHO. *Guidelines for Drinking-Water Quality*, 2nd ed.; WHO Press: Geneva, Switzerland, 1993.
3. Nicomel, N.R.; Leus, K.; Folens, K.; Van Der Voort, P.; Du Laing, G. Technologies for Arsenic Removal from Water: Current Status and Future Perspectives. *Int. J. Environ. Res. Public Health* **2016**, *13*, 62. [CrossRef] [PubMed]
4. Coudert, L.; Bondu, R.; Rakotonimaro, T.V.; Rosa, E.; Guittonny, M.; Neculita, C.M. Treatment of As-rich mine effluents and produced residues stability: Current knowledge and research priorities for gold mining. *J. Hazard. Mat.* **2020**, *386*, 121920. [CrossRef] [PubMed]
5. Mohan, D.; Pittman, C.U. Arsenic removal from water/wastewater using adsorbents—A critical review. *J. Hazard. Mater.* **2007**, *142*, 1–53. [CrossRef]
6. Vega-Hernandez, S.; Weijma, J.; Buisman, C.J.N. Immobilization of arsenic as scorodite by a thermoacidophilic mixed culture via As(III)-catalyzed oxidation with activated carbon. *J. Hazard. Mater.* **2019**, *368*, 221–227. [CrossRef]
7. Kowalski, K.P. Advanced arsenic removal technologies review. In *Chemistry of Advanced Environmental Purification Processes of Water*, 1st ed.; Søgaard, E.G., Ed.; Elsevier: Amsterdam, The Netherlands, 2014; pp. 285–337. [CrossRef]
8. Mandal, B.K. Changing concept of arsenic toxicity with development of speciation techniques. In *Handbook of Arsenic Toxicology*, 1st ed.; Flora, S.J.S., Ed.; Academic Press: Amsterdam, The Netherlands, 2015; pp. 179–201. [CrossRef]
9. Okibe, N.; Koga, M.; Sasaki, K.; Hirajima, T.; Heguri, S.; Asano, S. Simultaneous oxidation and immobilization of arsenite from refinery waste water by thermoacidophilic iron-oxidizing archaeon, *Acidianus brierleyi. Miner. Eng.* **2013**, *48*, 126–134. [CrossRef]
10. González-Contreras, P.A.; Weijma, J.; Buisman, C.J.N. Kinetics of ferrous iron oxidation by batch and continuous cultures of thermoacidophilic Archaea at extremely low pH of 1.1-1.3. *Appl. Microbiol. Biotechnol.* **2012**, *93*, 1295–1303. [CrossRef]
11. Li, S.W.; Sheng, G.P.; Cheng, Y.Y.; Yu, H.Q. Redox properties of extracellular polymeric substances (EPS) from electroactive bacteria. *Sci. Rep.* **2016**, *6*, 1–7. [CrossRef]
12. Lin, Z.Q.; Shao, W.; Xu, J.; Sheng, G.P. Accurately quantifying the reductive capacity of microbial extracellular polymeric substance by mediated electrochemical oxidation method. *Sci. Total Environ.* **2019**, *673*, 541–545. [CrossRef]
13. Sathishkumar, K.; Li, Y.; Sanganyado, E. Electrochemical behavior of biochar and its effects on microbial nitrate reduction: Role of extracellular polymeric substances in extracellular electron transfer. *Chem. Eng. J.* **2020**, *395*, 125077. [CrossRef]
14. González-Contreras, P.A. Bioscorodite: Biological Crystallization of Scorodite for Arsenic Removal. Ph.D. Thesis, Wageningen University and Research, Wageningen, The Netherlands, 2012.
15. Fujita, T.; Fujieda, S.; Shinoda, K.; Suzuki, S. Environmental leaching characteristics of scorodite synthesized with Fe(II) ions. *Hydrometallurgy* **2012**, *111*, 87–102. [CrossRef]
16. Robins, R.G.; Dove, P.M.; Rimstidt, J.D.; Nordstrom, D.K.; Parks, G.A. Solubility and stability of scorodite, $FeAsO_4 \cdot 2H_2O$; discussions and replies. *Am. Mineral.* **1987**, *72*, 842–855.
17. Singhania, S.; Wang, Q.; Filippou, D.; Demopoulos, G.P. Temperature and seeding effects on the precipitation of scorodite from sulfate solutions under atmospheric-pressure conditions. *Metall. Mater. Trans. B* **2005**, *36*, 327–333. [CrossRef]
18. Tanaka, M.; Sasaki, K.; Okibe, N. Behavior of sulfate ions during biogenic scorodite crystallization from dilute As(III)-bearing acidic waters. *Hydrometallurgy* **2018**, *180*, 144–152. [CrossRef]

19. González-Contreras, P.A.; Weijma, J.; Buisman, C.J.N. Arsenic immobilization by biological scorodite crystallization: Effect of high ferric concentration and foreign seeds. *Adv. Mater. Res.* **2009**, *71–73*, 629–632. [CrossRef]

20. Fitzpatrick, J.J. Insights from mathematical modelling into energy requirement and process design of continuous and batch stirred tank aerobic bioreactors. *Chemengineering* **2019**, *3*, 65. [CrossRef]

21. Tec-Caamal, E.N.; Rodríguez-Vázquez, R.; Torres-Bustillos, L.G.; Aguilar-López, R. Kinetic analysis via mathematical modeling for ferrous iron oxidation in a class of SBR-type system. *Chin. J. Chem. Eng.* **2019**, *27*, 2472–2480. [CrossRef]

22. Figueroa-Estrada, J.C.; Neria-González, M.I.; Rodríguez-Vázquez, R.; Tec-Caamal, E.N.; Aguilar-López, R. Controlling a continuous stirred tank reactor for zinc leaching. *Miner. Eng.* **2020**, *157*, 106549. [CrossRef]

23. Tec-Caamal, E.N.; Rodríguez-Vázquez, R.; Weijma, J.; Aguilar-López, R. Simulation platform for in-situ Fe(II) oxidation and bioscorodite crystallization in a one-step process for As(V) immobilization from acid wastewater. *Miner. Eng.* **2021**, *172*, 107170. [CrossRef]

24. Fujita, T.; Taguchi, R.; Abumiya, M.; Matsumoto, M.; Shibata, E.; Nakamura, T. Novel atmospheric scorodite synthesis by oxidation of ferrous sulfate solution. Part I. *Hydrometallurgy* **2008**, *90*, 92–102. [CrossRef]

25. Vega-Hernandez, S.; Weijma, J.; Buisman, C.J.N. Particle size control of biogenic scorodite during the GAC-catalysed As(III) oxidation for efficient arsenic removal in acid wastewaters. *Water Resour. Ind.* **2020**, *23*, 100128. [CrossRef]

26. PAQUES Technology. THIOTEQTM Scorodite. 2020. Available online: https://en.paques.nl/products/other/thioteqscorodite (accessed on 26 August 2022).

27. Okibe, N.; Koga, M.; Morishita, S.; Tanaka, M.; Heguri, S.; Asano, S.; Sasaki, K.; Hirajima, T. Microbial formation of crystalline scorodite for treatment of As (III)-bearing copper refinery process solution using *Acidianus brierleyi*. *Hydrometallurgy* **2014**, *143*, 34–41. [CrossRef]

28. Sheng, Y.; Kaley, B.; Bibby, K.; Grettenberger, C.; Macalady, J.L.; Wang, G.; Burgos, W.D. Bioreactors for low-pH iron(II) oxidation remove considerable amounts of total iron. *RSC Adv.* **2017**, *7*, 35962–35972. [CrossRef]

29. Pesic, B.; Oliver, D.J.; Wichlacz, P. An electrochemical method of measuring the oxidation rate of ferrous to ferric iron with oxygen in the presence of *Thiobacillus ferrooxidans*. *Biotechnol. Bioeng.* **1989**, *33*, 428–439. [CrossRef]

30. Kirby, C.S.; Thomas, H.M.; Southam, G.; Donald, R. Relative contributions of abiotic and biological factors in Fe(II) oxidation in mine drainage. *Appl. Geochem.* **1999**, *14*, 511–530. [CrossRef]

31. Xiao, Y.; Zhang, E.; Zhang, J.; Dai, Y.; Yang, Z.; Christensen, H.E.; Ulstrup, J.; Zhao, F. Extracellular polymeric substances are transient media for microbial extracellular electron transfer. *Sci. Adv.* **2017**, *3*, e1700623. [CrossRef]

32. González-Contreras, P.A.; Weijma, J.; Buisman, C.J.N. Bioscorodite crystallization in an airlift reactor for arsenic removal. *Cryst. Growth Des.* **2012**, *12*, 2699–2706. [CrossRef]

33. Mullin, J.W. *Crystallization*, 4th ed.; Butterworth-Heinemann: Oxford, UK, 2001. [CrossRef]

34. González-Contreras, P.A.; Weijma, J.; Buisman, C.J.N. Continuous bioscorodite crystallization in CSTRs for arsenic removal and disposal. *Water Res.* **2012**, *46*, 5883–5892. [CrossRef] [PubMed]

35. Mbamba, C.K.; Batstone, D.J.; Flores-Alsina, X.; Tait, S. A generalised chemical precipitation modelling approach in wastewater treatment applied to calcite. *Water Res.* **2015**, *68*, 342–353. [CrossRef] [PubMed]

36. Dove, P.M.; Rimstidt, J.D. The solubility and stability of scorodite, $FeAsO_4 \cdot 2H_2O$. *Am. Mineral.* **1985**, *70*, 838–844.

37. Tanaka, M.; Okibe, N. Factors to enable crystallization of environmentally stable bioscorodite from dilute As(III)-contaminated waters. *Minerals* **2018**, *8*, 23. [CrossRef]

38. Jarrett, A.M.; Liu, Y.; Cogan, N.G.; Hussaini, M.Y. Global sensitivity analysis used to interpret biological experimental results. *J. Math. Biol.* **2015**, *71*, 151–170. [CrossRef] [PubMed]

39. Sainte-Marie, J.; Cournède, P.H. Insights of global sensitivity analysis in biological models with dependent parameters. *J. Agric. Biol. Environ. Stat.* **2019**, *24*, 92–111. [CrossRef]

40. Vega-Hernandez, S.; Sánchez-Andrea, I.; Weijma, J.; Buisman, C.J.N. An integrated green methodology for the continuous biological removal and fixation of arsenic from acid wastewater through the GAC-catalyzed As(III) oxidation. *Chem. Eng. J.* **2021**, *421*, 127758. [CrossRef]

41. Barahona, S.; Herrera, E.; Jara, A.; Castro-Severyn, J.; Gallardo, K.; Fuentes, G.; Dorador, C.; Saavedra, C.; Remonsellez, F. Arsenopyrite Dissolution and Bioscorodite Precipitation by Acidithiobacillus ferrivorans ACH under Mesophilic Condition. *Minerals* **2022**, *12*, 520. [CrossRef]

42. Tanaka, M.; Hirajima, T.; Sasaki, K.; Okibe, N. Optimization of bioscorodite crystallization for treatment of As(III)-bearing wastewaters. *Solid State Phenom.* **2017**, *262*, 555–558. [CrossRef]

43. Vanlier, J.; Tiemann, C.A.; Hilbers, P.A.J.; van Riel, N.A.W. Parameter uncertainty in biochemical models described by ordinary differential equations. *Math. Biosci.* **2013**, *246*, 305–314. [CrossRef]

44. Orell, A.; Schopf, S.; Randau, L.; Vera, M. Biofilm Lifestyle of Thermophile and Acidophile Archaea. In *Biocommunication of Archaea*, 1st ed.; Witzany, G., Ed.; Springer: Cham, Switzerland, 2017; pp. 133–146. [CrossRef]

45. Sellke, T.; Bayarri, M.J.; Berger, J.O. Calibration of *p* values for testing precise null hypotheses. *Am. Stat.* **2001**, *55*, 62–71. [CrossRef]

46. Garcia-Rios, M.; De Windt, L.; Luquot, L.; Casiot, C. Modeling of microbial kinetics and mass transfer in bioreactors simulating the natural attenuation of arsenic and iron in acid mine drainage. *J. Hazard. Mater.* **2021**, *405*, 124133. [CrossRef]

47. Higashidani, N.; Kaneta, T.; Takeyasu, N.; Motomizu, S.; Okibe, N.; Sasaki, K. Speciation of arsenic in a thermoacidophilic iron-oxidizing archaeon, *Acidianus brierleyi*, and its culture medium by inductively coupled plasma–optical emission spectroscopy combined with flow injection pretreatment using an anion-exchange mini-column. *Talanta* **2014**, *122*, 240–245. [CrossRef]
48. Bertoldo, C.; Dock, C.; Antranikian, G. Thermoacidophilic microorganisms and their novel biocatalysts. *Eng. Life Sci.* **2004**, *4*, 521–532. [CrossRef]
49. Nemati, M.; Harrison, S.T.L. A comparative study on thermophilic and mesophilic biooxidation of ferrous iron. *Miner. Eng.* **2000**, *13*, 19–24. [CrossRef]